Chinese Chemical Letters 35 (2024) 109238

Contents lists available at ScienceDirect

Chinese Chemical Letters

journal homepage: www.elsevier.com/locate/cclet

Intelligent laser-induced graphene sensor for multiplex probing catechol isomers

Tian Cao, Xuyin Ding, Qiwen Peng, Min Zhang*, Guoyue Shi

School of Chemistry and Molecular Engineering, Shanghai Key Laboratory for Urban Ecological Processes and Eco-Restoration, East China Normal University, Shanghai 200241, China

ARTICLE INFO

Article history:
Received 7 June 2023
Revised 30 September 2023
Accepted 20 October 2023
Available online 27 October 2023

Keywords:
Laser-induced graphene
Phenolic pollutants
Electrochemical detection
Artificial neural network

ABSTRACT

Herein, we unveil the intelligent detection of multiple catechol isomers in complex environments utilizing both laser-induced graphene (LIG) and artificial neural network (ANN). The large scale-up manufacturing of LIG-based sensors (LIGS) with three-electrode configuration on polyimide (PI) is achieved by direct laser-writing and screen-printing technologies. Our LIGS shows excellent electrochemical performance toward catechol isomers, *i.e.*, hydroquinone (1,4-dihydroxybenzene, HQ), catechol (1,2-dihydroxybenzene, CT), and resorcinol (1,3-dihydroxybenzene, RC), with a low limit of detection (LOD) (CC, 0.079 μmol/L; HQ, 0.093 μmol/L; RC, 1.18 μmol/L). Moreover, the ANN model is developed for machine-intelligent to predict concentrations of catechol isomers under an interfering environment *via* a single LIGS. Using six unique parameters extracted from the differential pulse voltammetry (DPV) response, the machine learning-based regression provides a coefficient of correlation with 0.998 and is able to correctly predict the total and individual concentrations in complex river samples. Hence, this work provides a guide for the preparation and application of LIGS *via* facile and cost-efficient mass production and the development of an intelligent sensing platform based on the ANN model.

Catechol isomers, *i.e.*, hydroquinone (1,4-dihydroxybenzene, HQ), catechol (1,2-dihydroxybenzene, CC) and resorcinol (1,3-dihydroxybenzene, RC), are widely used in the pharmaceutical industry, cosmetics manufacturing, rubber antioxidant and other fields [1–5]. As highly toxic organic compounds for both human health and the environment, catechol isomers attract much attention regarding their sensitive and selective determination. However, due to the similarity in their structures and properties, it is fascinating and challenging to establish a method for the simultaneous detection of catechol isomers [6–9]. So far, various methods have been reported for the detection of catechol isomers, such as high-performance liquid chromatography coupled mass spectrometry (HPLC-MS), electrophoresis, and gas chromatography coupled mass spectrometry (GC-MS) [10–12]. Compared to these methods, electrochemical sensors are more suitable for detecting in-field and timely screening large samples due to their advantages of cost-efficiency, sensitivity, simplicity, and wide linear range [13–15]. These characteristics offer enormous potential for rapid and precise detection and assessment of catechol isomers in environmental samples.

Carbon materials possess various morphologies and tunable engineered properties, which have been widely applied in electrochemical sensors [16,17]. Numerous types of research showed that three-dimensional (3D) porous graphene could enhance electrochemical response, due to its large specific surface area and highly conductive pathways, stimulating adequate efficiency in charge transfer and mass transport [18,19]. Nevertheless, the methods of fabricating 3D graphene, *e.g.*, template-mediated assembly, chemical vapor deposition (CVD), and self-assembly, generally require complicated and environmentally unfriendly chemical synthesis or expensive instruments [20–23]. Moreover, electrochemical devices that utilized these materials commonly require additional binders or additives. The aforesaid reasons constrain their wide application in electrochemical sensing. Laser-induced graphene (LIG), as an emerging electrode material, can be created by directly laser-writing technology [24–31]. Combined with the merits of being free of chemical reagents, one-step processing, and simple patterning, this technology can advance a facile route to electronic devices such as sensing. Recently, LIG has been widely utilized in various aspects of electrochemical sensors for the detection of biomarkers, environmental pollutants, viruses and so on [32–37]. Thus, the construction of disposable and high-performance LIG sensors would provide a viable strategy for on-site and large-scale monitoring of biochemicals (*e.g.*, catechol).

* Corresponding author.
E-mail address: mzhang@chem.ecnu.edu.cn (M. Zhang).

https://doi.org/10.1016/j.cclet.2023.109238
1001-8417/

Another challenge in sensor practical application is the lack of innovative strategies for selective detection of multiple targets under varying environments, due to the cross interferences. Regression analysis, a subfield of machine learning (ML) algorithm, is a powerful tool for environmental monitoring incorporated with sensing techniques to address cross-interferences [38,39]. Especially, artificial neural network (ANN) for regression analysis, a vital ML algorithm, has recently attracted increasing interest in analytical chemistry because of the ability to model either linear or non-linear systems, the features of learning, and ease of implementation [40–42]. For example, the ANN model combined with an electrochemical sensor has been used to accurately measure the concentrations of naphthalene acetic acid [43]. However, most ML-supported electrochemical sensors only addressed the concentration prediction of a single analyte or accomplished multiple analyte concentration predictions *via* constructing a sensor array to obtain multidimensional features. Consequently, multi-feature extraction of signals as fingerprint information is an effective strategy to realize multi-target detection. Meanwhile, it is difficult to directly show the parameter relationship behind the model, resulting in ANN only needing input and output variables like "Black box" [44]. Therefore, a local feature importance measurement can be introduced to better comprehend the relationships among features and visualize how changes in features affect the model performances, *via* two visual tools: partial dependence plots (PDPs) and Shapley Additive exPlanations (SHAPs) [45,46].To date, a single LIG sensor integrated with both ANN algorithm and multi-feature extraction has not been explored for precisely and simultaneously detecting the total and individual concentration of 3 catechol isomers.

Herein, a single LIG sensor without any active-materials modification, integrated with both ANN algorithms and multi-feature extraction has been unveiled for intelligently detecting the total concentration and individual concentration of catechol isomers in complex samples (Scheme 1). As a proof concept, a LIG-based sensor (LIGS) with a three-electrode configuration was large-scale fabricated *via* the laser-writing technology assisted with screen-printing technology. The designed low-cost and high-performance LIGS was then used to selectively monitor three common phenol pollutants, *i.e.*, catechol isomers including catechol (CC), resorcinol (RC), hydroquinone (HQ), through differential pulse voltammetry (DPV). To overcome the cross-interferences and offer a quantitative and accurate detection of 3 catechol isomers, 6 features (response change and peak area) were exacted from the obtained DPV responses to establish the ANN-supported algorithm. Besides, PDPs and SHAPs were utilized to analyze and visualize the relationship between the input parameters on the output results in the established algorithm model. Such smart LIGS could be a transformative approach for the *in-situ* analysis of phenolic compounds in the environment, paving the pathway of precise and real-time environmental monitoring in the future.

The pattern of the LIG-based three-electrode was designed on a computer with the vector graphics software CorelDraw. Laser rastering settings are as follows: laser power 10% (2.5 W) and speed of 15% (150 mm/s). The LIGS with three-electrode configuration was prepared on a commercially available substrate polyimide (PI) sheet, in which two unmodified LIG electrodes respectively act as the working and counter electrode, the other LIG electrode screen-printed with Ag/AgCl paste acts as the reference electrode (Fig. S1 in Supporting information). Details on the fabrication of LIGS are given in Text S3 (Supporting information).

All measurements were carried out on a CHI660E electrochemical workstation (Shanghai Chenhua Instruments Co., Ltd., China) with the LIGS. To explore the preparation condition of the LIGS and the effect of applied strain on electrochemical behavior, the cyclic voltammetry (CV) measurement was performed in 0.1 mol/L KCl solution containing 1.0 mmol/L $K_3[Fe(CN)_6]^{3-/4-}$ over the voltage range between −0.2 V and +0.6 V. The electroactive sensing of

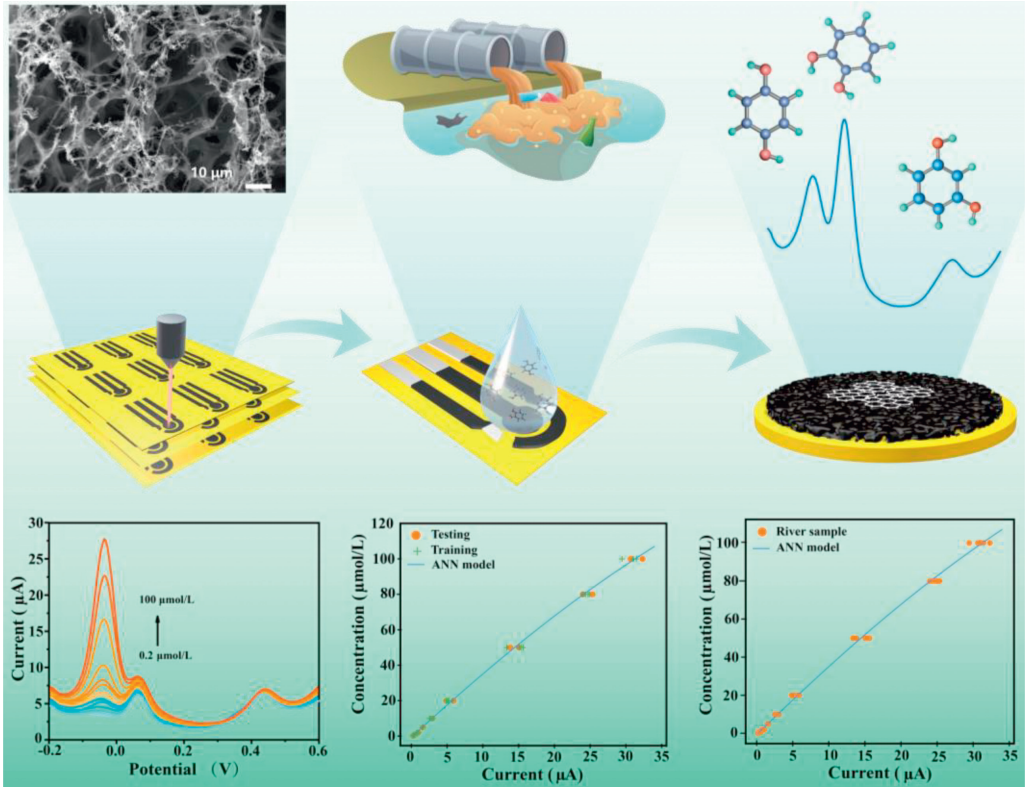

Scheme 1. Illustration of intelligent LIG-based sensor for multiplex detection of catechol isomers.

catechol isomers was carried out from −0.2 V to +0.6 V in the PBS solution (0.1 mol/L, pH = 7) using the differential pulse voltammetry (DPV) method with the scan rate of 0.05 V/s. The river sample was collected from Huangpu River, filtered through a 0.45 μm filter to remove impurities, and diluted with 0.1 mol/L PBS (pH 7.0) solution (v:v = 1:1) to adjust the pH value. The standard addition protocol was used to analyze catechol isomers in the real samples. Certain concentrations of CC, HQ, and RC were added to the prepared samples, respectively. Moreover, the recoveries were tested according to the equation: Recovery (%) = concentration tested/concentration added × 100%.

Fig. 1A is the simplified diagram of the mass preparation of LIGS. The transformation of PI to LIG is a photothermal process associated with the localized high temperature, in which the chemical bonds in the precursor will be broken and recombined. With the rapid liberation of gaseous products, LIG exhibits the appearance of a foam structure. As shown in Fig. 1A(a), the predesigned pattern was quickly engraved to the PI surface to form highly conductive LIG by laser scribing. Then, silver slurry and silver chloride slurry were quickly coated by screen-printing technology so as to mitigate wear on the sensor and increase the conductivity. Details on the fabrication process are given in Fig. S2 (Supporting information). The patternable and efficient manufacturing process of LIGS illuminates a cost-effective pathway for developing graphene-based electrochemical devices.

Laser power and scan speed are the significant factors for the micro-morphologies and electroanalytical characteristics of porous LIG. The PI sheet was not carbonized or only partially carbonized at low power, and the more porous graphene formed as the power increased (Fig. S3 in Supporting information). A morphology of LIG with long and messy fiber was formed on the surface at considerably higher power. This kind of LIG is not favorable for electroanalysis on account of looser structures leading to higher resistance. Considering the CV responses of LIGS at different powers (Fig. S4A in Supporting information), 2.5 W was chosen as the optimal power. The influence of scan speed was also investigated. When the scan speed was too fast, the structure of LIG was flocculent and prone to falling. When the scan speed was too slow, PI cannot be converted to porous graphene. The corresponding CV responses also verified the influence of the scan speed (Fig. S4B in Supporting information). Thus, 150 mm/s was set as the optimal speed.

The morphology was characterized by scanning electron microscopy (SEM). The top-view SEM images of LIG exhibited the abundant of edge-plane and the appearance of a honeycomb with a porous structure owing to the rapid liberation of gaseous products during direct laser writing (Figs. 1B and C). The available edge-plane sites on the surface-enhanced the electron transfer behavior of LIG. The 3D porous morphology can also offer a highly accessible electrochemical active area.

As shown in Fig. 1D, the contact angle of LIG was about 63°, demonstrating that the surface of LIG was relatively hydrophilic at 2.5 W power. The surface of LIG gradually became more hydrophobic with increasing laser power (Fig. S5 in Supporting information), because of the deepening degree of carbonization and the reduction of oxygen-containing groups. Proper hydrophilicity is beneficial for the electrolyte accessibility to the electrode surfaces. In this respect, it is reasonable to choose the optimal laser power at 2.5 W.

The XRD pattern presented a sharp peak at $2\theta = 25.9°$ with an interlayer spacing of 0.34 nm (Fig. 1E), suggesting a high degree of graphitization. The small peak can be observed at $2\theta = 42.9°$ matched the (100) reflections, attributing to an sp^2 in-plane structure, which is in agreement with the reported literature.

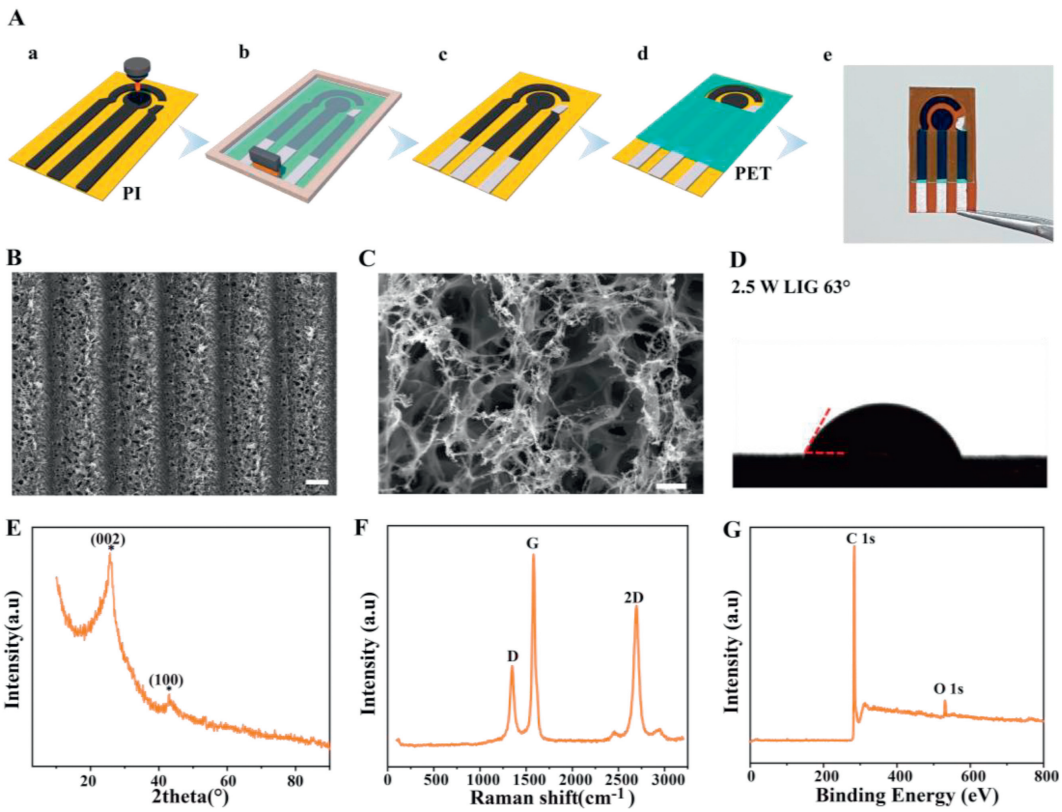

Fig. 1. (A) The fabrication of LIGS: (a) CO_2 laser irradiation, (b) screen-printing of silver and silver chloride paste, (c) drying and curing, (d) covering pre-patterned PET mask and (e) the image of LIGS. (B) SEM image of the porous LIG prepared at 2.5 W power and 150 mm/s speed (30 μm). (C) Amplified SEM image of LIG surface (10 μm). (D) Contact angle of LIG prepared at 2.5 W power and 150 mm/s speed. (E) XRD pattern, (F) Raman spectrum, and (G) XPS survey of LIG.

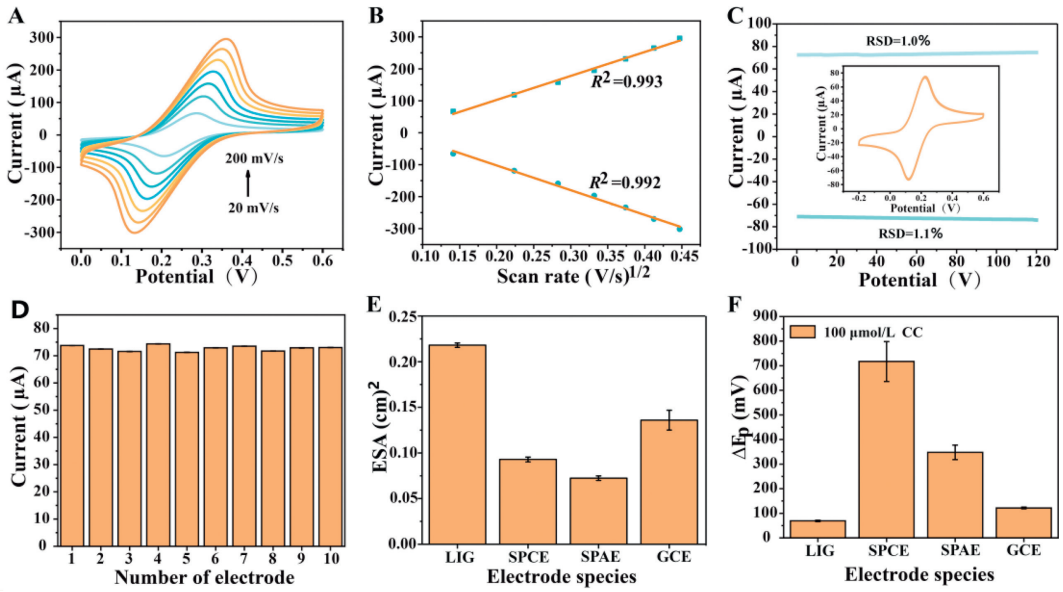

Fig. 2. Electrochemical characterization of the LIGS: (A) cyclic voltammograms at 20–200 mV/s in 5 mmol/L $[Fe(CN)_6]^{3-/4-}$ containing 0.1 mol/L KCl. (B) *Randles-Sevcik* plot; (C) the stability of successive 150 cycles of CV scans at LIGS. (D) The reproducibility of fabricated LIGS with different 10 batches in 5 mmol/L $[Fe(CN)_6]^{3-/4-}$ containing 0.1 mol/L KCl. (E) The calculated electroactive surface area (ESA) of different electrode species (the semicircle diameter of the working electrode both are 0.3 cm). (F) The peak-to-peak separation (ΔE_p) of different electrode species in 0.1 mmol/L PBS challenged with 100 μmol/L CC.

Raman spectroscopy was used to investigate the characterization of LIG (Fig. 1F). Three main peaks D (1359 cm^{-1}), G (1581 cm^{-1}), and 2D (2725 cm^{-1}), confirmed the graphene was formed by lasering technology. The D and 2D peaks can be attributed to the primary in-plane and second-order in-plane vibrations, respectively. Similarly, the G peak is characteristic of the sp^2-bonded carbon atoms, which is more intense compared to the D peak. And the low I_D/I_G ratio of 0.38 revealed the highly crystalline structure of graphene. The I_{2D}/I_G calculated in this study was around 0.78, correlating with the formation of graphene multilayers. The chemical compositions of LIG were analyzed by X-ray photoelectron spectroscopy (XPS) (Fig. 1G). A strong XPS signal was obtained from the carbon (C) C 1s peak and the oxygen (O) O 1s peak. The C/O ratio of 9:1 indicated a high degree of carbonization of PI after lasering, which was also verified from the energy dispersive spectrometer (EDS) images (Fig. S6 in Supporting information).

The electroactive surface area (ESA) was calculated using the *Randles–Sevcik* equation (Eq. S1 in Supporting information) by recording the anodic and cathodic current peaks at varying scan rates (Fig. 2A). The average ESA of LIG was calculated to be 0.2212 cm^2, which was almost three times to the actual geometric surface area of working electrode (0.071 cm^2). This self-supporting porous architecture offers a large specific surface area and is favorable for electrochemical sensing. Additionally, the peak current *vs.* the square root of the scan rate behaved linearly, revealing that the electrochemical process was controlled by diffusion (Fig. 2B). The cycle stability of LIGS was studied by changes of the $[Fe(CN)_6]^{3-/4-}$ redox couple (Fig. 2C). The peaks of oxidation and reduction at LIGS with continuous 150 cycles of CV scans had no observable changes; the relative standard deviation (RSD) values were 1.0% and 1.1%, manifesting the scan stability of LIGS. Furthermore, the LIGS was tested every day, retaining 98.75% and 98.91% initial redox peak currents after 15 days; the RSD values were 0.43% and 0.35% (Fig. S7 in Supporting information), demonstrating that the LIGS has good storage stability and lifetime. Similarly, the corresponding current values of 10 different batches of LIGS showed no significant changes of the $[Fe(CN)_6]^{3-/4-}$ redox couple and the RSD of current was 1.32% (Fig. 2D), suggesting that the LIGS has good reproducibility and the reliability of the preparation process. Then the electrochemical performance of LIGS was compared with conventional sensors of GCE, SPCE, and SPAE. The ESA of different sensors was calculated under the same conditions. LIGS has more outstanding ESA thanks to its honeycomb morphology (Fig. 2E). Electrochemical behaviors challenged with catechol were respectively recorded by CV at the SPCE, SPAE, GCE and LIGS in 0.1 mol/L PBS (pH 7.0). As indicated in Fig. 2F, there was a meaningful decrease in the peak-to-peak separation ($\Delta E_p = E_{pa} - E_{pc}$) on the LIGS, illustrating that a fast electron transfer occurred at the LIGS. The results revealed that the anodic peak potential of CC in the LIGS was shifted to the negative potential values and the corresponding current values of CC far exceeded other electrode species (Fig. S8 in Supporting information). This can be explained by the high porosity of the LIG working electrode as well as the graphene-like structure defects to assure fast electron mobility at the interface-electrolyte/LIG sensing area, thus improving target analytes to electrode mass transport/binding. LIGS significantly improved the electrochemical performance and changed the redox behavior of the analytes compared to conventional electrodes.

An estimate of the cost per unit was performed accounting for the cost of all materials involved, including the PI sheet, the silver conductive ink used for electrical contacts, and the PET film. The overall cost of materials was 0.15 $/unit. Even considering the costs involved in the facilities and equipment, the overall final cost of the LIGS should be much lower than the typical ~2.5 $/unit of the commercially available SPCE or SPAE, and ~100 $/unit GCE (Table S2 in Supporting information). This highlights the excellent features of LIGS that showed better electrochemical performance than the commercially available sensors, with the advantage of being less expensive and produced by lasering that allows freedom of design with a high resolution. This system is well suited for mass production outside of the cleanroom, and it would have broad application prospects.

Using the excellent conductivity and high porosity of LIG, the prepared LIGS were used for the simultaneous detection of three isomers of catechol. The performance of detecting these isomers of catechol by LIGS was investigated. The scan rate is an important parameter, which affects mass transport and electron transfer.

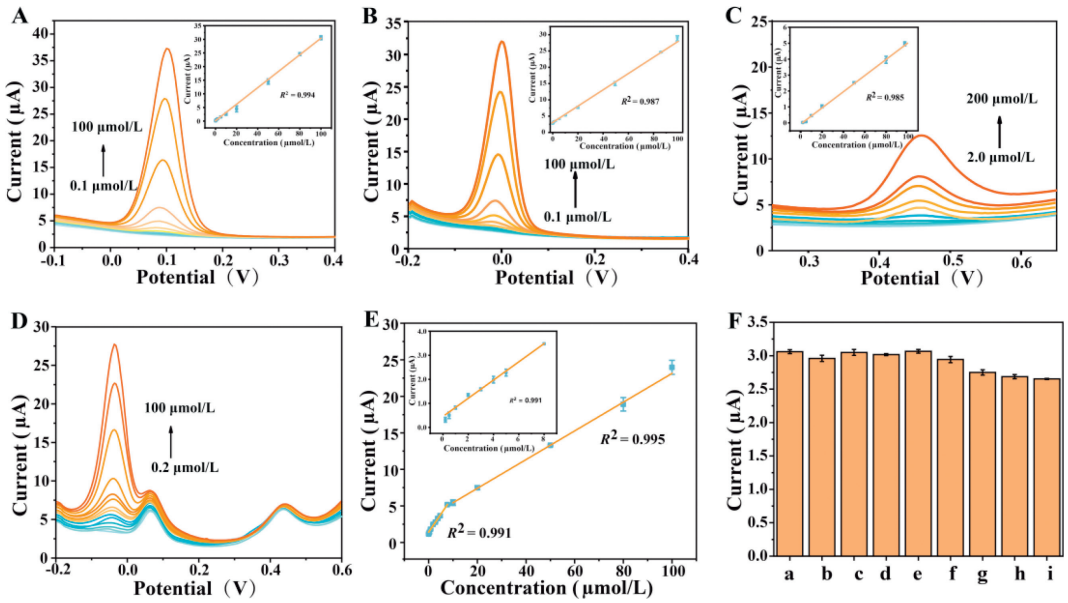

Fig. 3. Electrochemical detection of CC, HQ, and RC using the LIGS. DPV responses at different concentrations of (A) CC, (B) DA, and (C) RC in 0.1 mol/L PBS (pH 7.0). Insets: plots of each analyte's oxidation peak current density *versus* concentration. Linear fitting is used to determine the sensitivity of the electrodes for each analyte. (D) DPV responses at LIGS for various concentrations of HQ (0.2–100 μmol/L) containing CC (20 μmol/L) and RC (50 μmol/L), (E) the corresponding calibration plot. (F) The bar graph of relative error of LIGS in (a) 10 μmol/L CC and the additional presence of 100-fold excess of various compounds, *i.e.*, (b) $FeCl_3$, (c) $Cu(SO_4)_2$, (d) $NiCl_2$, (e) $Zn(NO_3)_2$, (f) glucose and uric acid, and 10-fold excess (g) ciprofloxacin, (h) tetracycline, and (i) erythromycin.

Figs. S9A-C (Supporting information) show CV responses recorded at different scan rates from 20 mV/s to 200 mV/s in 0.1 mol/L PBS (pH 7.0) containing 100 μmol/L of CC, HQ and RC. The plots showed good linearity (Figs. S9D-F in Supporting information), with the linear regression equation for CC, HQ and RC as Text S3 (Supporting information) expressed. These linear equations indicate that the electro-oxidation of catechol isomers at the LIGS are representative adsorption-controlled process. As shown in Fig. S9C (Supporting information), there is no reduction peak of RC. Due to the difference in the energy between the highest and lowest occupied molecular orbitals being large, the electrochemical redox process of RC must take place at a higher potential. Therefore, the electrochemical redox process of RC is irreversible. In addition, the mechanism of electrochemical redox of RC is still unclear due to its particularity. According to previous research, there are two mechanisms to explain the redox process (Figs. S11B and C in Supporting information).

The effect of pH on the electrochemical signal of LIGS was investigated in the range of pH 3–11 in 0.1 mol/L PBS containing 200 μmol/L CC. As shown in Fig. S10 (Supporting information), with the pH increasing the current of the analyte catechol isomers first increased and then decreased. Because catechol isomers could easily deprotonate when they are in an alkaline atmosphere. Meanwhile, the potential gradually shifted to the negative direction, implying the involvement of protons in the oxidation process. As the literature states that most phenolic compounds tend to reach their highest electro-oxidation in neutral pH media. Hence, pH 7.0 was selected for further experiments. The peak potentials showed a linear relationship against the pH, with regression equations for CC, HQ and RC as Text S4 (Supporting information) expressed. From the Nernst equation (Eq. S2 in Supporting information), the ratio of m/n was calculated to be 0.864 for CC, 1.08 for HQ and 0.949 for RC, indicating that an equal number of electrons and protons were involved in the electrochemical oxidation process. Based on this, the detection mechanism is illustrated in Fig. S11 (Supporting information). The hydroxyl group of the catechol isomers is electrocatalytically oxidized to form quinones, which is a 2-electron and 2-proton process. The DPV response of CC (Fig. 3A, 0.1–100 μmol/L), HQ (Fig. 3B, 0.1–100 μmol/L) and RC (Fig. 3C, 2.0–200 μmol/L) in pH 7.0 PBS at 50 mV/s scan rate was recorded. The results revealed that the current increases linearly with increasing concentrations of CC, HQ and RC. The calculated linear regression equations were as follows: $I_p = 0.30268C_{CC} + 0.13671$ ($R^2 = 0.994$); $I_p = 0.25914C_{HQ} + 0.05774$ ($R^2 = 0.987$); $I_p = 0.05073C_{RC} - 0.07725$ ($R^2 = 0.985$), and the limit of detections were calculated ($S/N = 3$) to be 0.079 μmol/L for CC, 0.093 μmol/L for HQ and 1.18 μmol/L for RC, respectively. The performance comparison of the present work and some recently reported electrodes for the determination of catechol isomers was summarized in Table S3 (Supporting information). The table clearly shows that the LIGS has relatively low detection limits without any further sensor modifications, which usually require complicated and time-consuming chemical synthesis.

The selectivity factor was then used for evaluating the selectivity of the LIGS. It could be observed clearly that the currents had nothing tremendous change upon challenged with a 100-fold concentration of some ions and molecules (data change below 3%, Fig. 3F), indicating outstanding selectivity and anti-interference properties of LIGS. The repeatability and reproducibility of LIGS for voltammetric responses to 100 μmol/L CC were also evaluated (Fig. S12 in Supporting information). The same LIGS was tested ten times with an RSD of 3.13%, indicating that it has satisfactory repeatability. The good reproducibility of LIGS was confirmed, with RSDs of 3.26% among ten independent electrodes.

For simultaneous determination, the calibration curves of HQ and CC all showed a two-segment feature. As illustrated in Figs. 3D and E, the oxidation peak current of HQ increased linearly with its concentration range from 0.2 μmol/L to 100 μmol/L in the presence of 20 μmol/L CC and 50 μmol/L RC, and the oxidation peak current of RC remained nearly constant as the concentration of HQ increased. Similarly, Fig. S13 (Supporting information) presented the trend of CC from 0.2 μmol/L to 100 μmol/L in the presence of 20 μmol/L HQ and 100 μmol/L RC and the trend of RC from 3.0 μmol/L to 200 μmol/L in the presence of 5 μmol/L HQ and 5 μmol/L CC, suggesting that the potential of CC, HQ and RC does

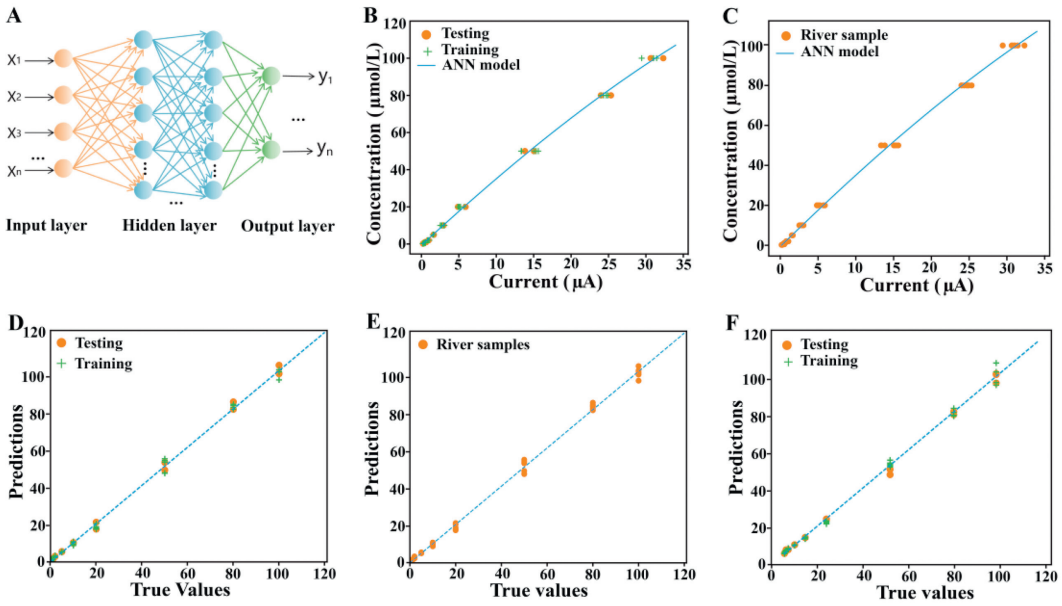

Fig. 4. (A) Summary diagram of neural network algorithm. Fitting analysis of ANN model in (B) pH 7 PBS, and (C) river sample. Performance of ML algorithms in predicting the concentration of CC in (D) pH 7 PBS, (E) river sample, and (F) concentration of HQ in pH 7 PBS.

not interfere with each other when simultaneously detection at LIGS. The regression equations for HQ and CC were exhibited as Text S5 (Supporting information). The LOD values were estimated to be 0.1025 μmol/L for HQ and 0.0853 μmol/L for CC, respectively. The two sectional linearity may be due to the following reason, at low analyte concentration (<10 μmol/L), the LIGS is rich in unoccupied active sites, meanwhile, a rapid sensing response can be reached by a fast depletion of the analyte. Contrarily, at higher analyte concentrations, the electrode has less sensitive due to contamination caused by derivatization products occupying more active sites.

Finally, in order to assess its practical application, the standard addition method was employed to the determination of CC, HQ and RC in river samples, and the recoveries and the RSD were 90.6%–110.8% and 3.41%–5.53%, respectively (Table S4 in Supporting information). Compared with the traditional high-performance liquid chromatography (HPLC) method, the concentration of the river sample detecting by LIGS was closer to the added value, indicating that LIGS had higher detection sensitivity. This result shows that the proposed LIGS is promising in real sample analysis.

Obviously, the linearity of phenolic pollutants in complex mixed systems or in river water samples is significantly different. Signal crosstalk and impurity adsorption will affect the accurate detection of phenolic pollutants. Therefore, how to achieve accurate concentration monitoring in complex environments is a challenge. This work provides a new strategy to deal with signal crosstalk in complex environments by using powerful machine algorithms. ANN inspired by the biological neurons to simulate the neural operation of our human brain is one important of the algorithms of ML. It is generally composed of an input layer, one or more hidden layers and an output layer, and they are linked together by simple layers of neurons and operate in parallel. In this work, the ANN models consisted of three layers: (1) the features extracted from electrochemical sensors as the input layer; (2) the hidden layers containing multiple neurons; (3) the output layer representing a concentration of analyte (Fig. 4A). The obtained data after disrupting the order randomly is divided into two parts to establishing model: 70% of data was set for training the model and 30% of data was set for testing the model. Different networks were trained to achieve the optimum structure of the model function, and then the accuracy of the established model was verified by the training set. As illustrated in Fig. 4B, the ANN model for predicting the concentration of CC was successfully determined avoiding overfitting. And the model is still feasible in complex river sample as Fig. 4C shown. Meanwhile, RMSE, MAE, R^2, and MSE were used to evaluate the training set and the prediction set, and the results were shown in the Table S5 (Supporting information). It could be seen that whether in the training set or the prediction set, both RMSE, MSE and MAE of the model were relatively small, which were 1.47–1.7708, 2.1615–3.25 and 1.0408–1.1728, respectively, and the R^2 values were both above 0.99. This indicated that ANN for the regression analysis was feasible and had great performance. Besides, it could be observed that R^2 values of the ANN method (0.997) was better than the simple linear regression (0.994) (Table S5), manifesting that ANN model could better deal with the relationship between current and concentration. Figs. 4D–F and Fig. S13 (Supporting information) demonstrated the comparative diagram of the obtained predicted and experimental values for each network training and testing. We could clearly notice that the values are almost all on the diagonal, revealing that predicting values were considerably approximation to the true experimental concentration in both PBS and river samples at different concentrations of CC, HQ and RC. The established ANN model can accurately monitor the concentration of individual catechol isomers at LIGS.

However, the relationship between current response and concentration is variable due to adsorption competition, cross interference of signal, and complex actual environment. The simple ANN regression model established above is still not enough to overcome the basic limitations of simultaneous detection of isomer concentration in a mixed environment. Therefore, we propose a model that is closer to the real situation by mining the characteristic values between the sensor response and concentration from a large amount of data. To capture the more clustering features of the DPV response, the three current responses and three peek areas related to concentration were picked as characteristic response values for participating in modeling (Fig. 5A). The model built with six eigenvalues has higher R^2 values and lower MAE, RMSE and MSE than the model with only three eigenvalues (Fig. 5B). It is proved that the more eigenvalues, the more conducive to establishing the ANN model with better performance. In addition to the total concentra-

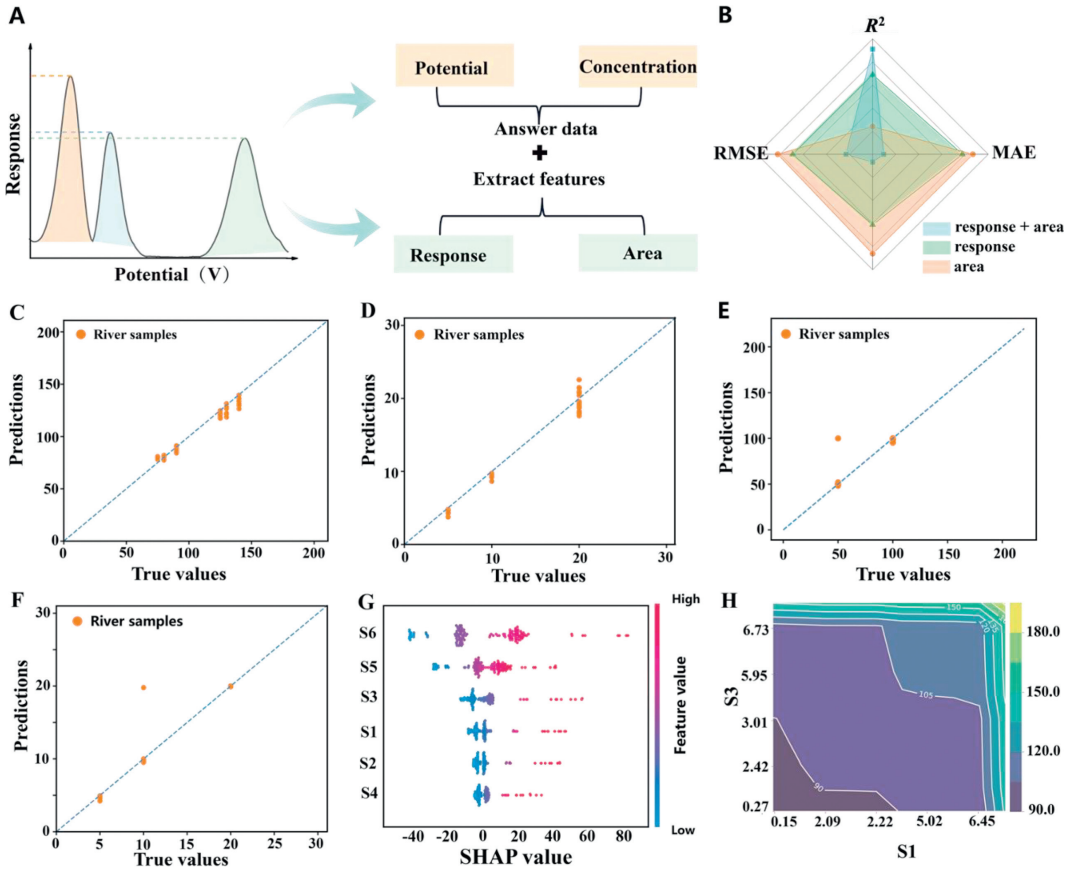

Fig. 5. (A) Schematic illustration of the data preparation for ANN-assisted classification. (B) Radar chart of model computational data for a different number of features. (C) Performance of ANN algorithms in predicting the total concentration of catechol isomers in pH 7 PBS. And the Performance of ANN algorithms in predicting the concentration of (D) CC, (E) HQ, and (F) RC in river samples, respectively. (G) Feature density scatter plot of six eigenvalues. (H) Partial Dependence Plots for features S1 and S3.

tion, the concentration of individual isomers can also be predicted in a complex mixed environment. All predicting values were almost on the diagonal (Figs. 5C–F and Fig. S18 in Supporting information). And the result got from the ANN model is that R^2 and MAE are about 0.989–0.998, 1.0521–1.8165 (Table S6 in Supporting information), indicating that the model has excellent performance and can be detected catechol isomers in practical samples. To sum up, the ANN model provides accurately predicted ability and realizes intelligent output.

As machine learning systems become more ubiquitous, methods for understanding and interpreting these models also become increasingly significant. In complex environments, the contribution of each characteristic value to the final concentration prediction is different due to the different degrees of influence from various aspects. In addition, as the artificial neural network model is like a black box, it can only see the results but cannot explore how the dependent variables affect the final results. Therefore, interpretable and explainable AI/ML models are now in high demand in chemical analysis. The SHAPs and PDPs are popular tools to enhance the interpretability of model decisions. As shown in Fig. 5G, the ranking of the 6 features was based on the average absolute values of SHAP representing the degree of contribution to the model. And the redder the color, the larger the value of the feature itself; the more dispersed the values, the greater the impact. Combined with Figs. S19 and S20 (Supporting information), the characteristic value of S6, that is, the peak area value of RC, contributes the most, because RC may be more affected by the environment, is difficult to oxidize, and has the lowest current response value. Fig. 5H shows the prediction results of any combination of S1 and S3 features, and Fig. S21 (Supporting information) shows the prediction results of any combination of S1 and other characteristic values. The results show that the degree of interaction increases with the increase in concentration. Moreover, the influence of different eigenvalues on each other is different, and the influence degree of eigenvalues with higher contribution values is also greater. This may be because the three isomers have different competitive abilities of adsorption on the electrode due to their different degree of electrochemical oxidation.

In conclusion, the ANN-based regression model established in this work has the potential to detect the concentration of three catechol isomers in complex actual water samples. Compared with the previous method of using a machine algorithm to establish a voltammetry regression model, we further innovated the model establishment method. First, we choose as many concentration-related eigenvalues as possible to build a model that is closer to the actual concentration. Secondly, based on model establishment, we use SHAPs and PDPs to explain the established model.

In summary, we have proposed a new strategy for monitoring catechol isomers under complex environments *via* the modification-free LIGS and ML based on an ANN model. Firstly, the combination of laser-induced and screen-printing processes successfully accomplished rapid mass production of binder-free electrodes. We systemically optimized and characterized the LIGS, showing that it has more excellent electrochemical performances over the conventional SPCEs, SPAEs and GCE. These advantages ensure the relatively fast electron transfer and readily accumulation of target analyte in distinguishing and detecting three catechol isomers with low detection limits (0.093, 0.079, and 1.18 μmol/L for HQ, CC, and RC, respectively). Besides, an ANN model was developed for machine intelligent prediction using a single LIGS, which

showed extraordinary accuracy for predicting the total concentration of catechol isomers and individual isomers. The predicted values of the output were compared with experimental values and the results showed that they were in great agreement with each other with an R^2 of above 0.99. The excellent electrochemical performance of the LIGS integrated with the reliable ANN algorithm proves the feasibility and detectability of the method for cost-effective, simple, and trace detection of hazardous phenolic substances regarding the safety of environments and humans.

Declaration of competing interest

The authors declare that they have no known competing financial interests or personal relationships that could have appeared to influence the work reported in this paper.

Acknowledgments

This work was supported by the National Natural Science Foundation of China (Nos. 22274053 and 22274051), and the Shanghai Municipal Science and Technology Major Project ("Beyond Limits Manufacture").

Supplementary materials

Supplementary material associated with this article can be found, in the online version, at doi:10.1016/j.cclet.2023.109238.

References

[1] H. Huang, Y. Chen, Z. Chen, et al., J. Hazard. Mater. 416 (2021) 125895.
[2] K.S. Ranjith, A.T. EzhilVilian, S.M. Ghoreishian, et al., J. Hazard. Mater. 421 (2022) 126775.
[3] R. Huang, D. Liao, S. Chen, J. Yu, X. Jiang, Sens. Actuators B: Chem. 320 (2020) 128386.
[4] Y.L. Qi, Y. Cao, X.T. Meng, et al., Sens. Actuators B: Chem. 279 (2019) 170–176.
[5] K. Chetankumar, B.E. Kumara Swamy, T.S. Sunil Kumar Naik, J. Mater. Sci.: Mater. Electron. 31 (2020) 19728–19740.
[6] J.S. Arya Nair, S. Saisree, K.Y. Sandhya, Analyst 147 (2022) 2966–2979.
[7] R. Huang, S. Chen, J. Yu, X. Jiang, Ecotoxicol. Environ. Saf. 184 (2019) 109619.
[8] Y. Zhang, G.M. Zeng, L. Tang, et al., Biosens. Bioelectron. 22 (2007) 2121–2126.
[9] L. Chen, Y. Tang, K. Wang, C. Liu, S. Luo, Electrochem. Commun. 13 (2011) 133–137.
[10] S.C. Moldoveanu, M. Kiser, J. Chromatogr. 1141 (2007) 90–97.
[11] G. Marrubini, E. Calleri, T. Coccini, et al., Chroma 62 (2005) 25–31.
[12] Z.M. Li, Y.C. Xi, A.Q. Zhao, et al., Anal. Bioanal. Chem. 412 (2021) 3541–3550.
[13] X. Xie, D.P. Wang, C. Guo, et al., Anal. Chem. 93 (2021) 4916–4923.
[14] X. Wang, G. Liu, Y. Qi, et al., Anal. Chem. 91 (2019) 12006–12013.
[15] K. Venkatesh, B. Muthukutty, S.M. Chen, et al., J. Hazard. Mater. 405 (2021) 124096.
[16] P. Nayak, N. Kurra, C. Xia, H.N. Alshareef, Adv. Electron. Mater. 2 (2016) 1600185.
[17] W. Yang, K.R. Ratinac, S.P. Ringer, et al., Angew. Chem. Int. Ed. 49 (2010) 2114–2138.
[18] W. Li, C. Tan, M. Lowe, H. Abruna, D. Ralph, ACS Nano 5 (2011) 2264.
[19] S. Banerjee, J. Shim, J. Rivera, et al., ACS Nano 7 (2013) 834–843.
[20] J. Zeng, X.X. Ji, Y.H. Ma, et al., Adv. Mater. 30 (2018) 1705380.
[21] S. Ullah, M. Hasan, H.Q. Ta, et al., Adv. Funct. Mater. 29 (2019) 1904457.
[22] J. Zhou, X. Wu, Y. Chen, et al., Adv. Funct. Mater. 32 (2022) 2105879.
[23] R. Zhao, K. Li, R. Liu, et al., J. Mater. Chem. A 5 (2017) 19098–19106.
[24] J. Lin, Z. Peng, Y. Liu, et al., Nat. Commun. 5 (2014) 5714.
[25] L. Huang, J. Su, Y. Song, et al., Nano-Micro Lett. 12 (2020) 157.
[26] R. Ye, D.K. James, J.M. Tour, Adv. Mater. 31 (2019) 1803621.
[27] Z. Wan, N.T. Nguyen, Y. Gao, Q. Li, Sustain. Mater. Technol. 25 (2020) e00205.
[28] W.J. Yu, W.W. Zhao, S.P. Wang, et al., Adv. Mater. 35 (2023) 2209545.
[29] W.W. Zhao, W.J. Yu, Y. Jiang, et al., Nano Energy 100 (2022) 107477.
[30] Y.Y. Peng, W.W. Zhao, F. Ni, et al., ACS Nano 15 (2021) 19490–19502.
[31] L. Ge, Q. Hong, H. Li, et al., Adv. Funct. Mater. 29 (2019) 1904000.
[32] A. Ghanam, A.A. Lahcen, T. Beduk, et al., Biosens. Bioelectron. 168 (2020) 112509.
[33] F. Zhao, J. He, X. Li, et al., Biosens. Bioelectron. 170 (2020) 112636.
[34] U. Rajaji, P.S. Ganesh, S.Y. Kim, et al., ACS Appl. Nano Mater. 5 (2022) 3252–3264.
[35] Y. Yang, Y. Song, X. Bo, et al., Nat. Biotechnol. 38 (2020) 217–224.
[36] R.R.A. Soares, R.G. Hjort, C.C. Pola, et al., ACS Sens. 5 (2020) 1900–1911.
[37] R.M. Torrente-Rodríguez, H. Lukas, J. Tu, et al., Matter 3 (2020) 1981–1998.
[38] L. Fu, Y.G. Wang, Environ. Sci. Technol. 45 (2011) 1481–1489.
[39] A. Mistry, A.A. Franco, S.J. Cooper, S.A. Roberts, V. Viswanathan, ACS Energy Lett. 6 (2021) 1422–1431.
[40] X.Y. Lu, P. Liu, K. Bisetty, et al., J. Electroanal. Chem. 920 (2022) 116634.
[41] P. Puthongkham, S. Wirojsaengthong, A. Suea-Ngam, Analyst 146 (2021) 6351–6364.
[42] X. Zhu, L. Liu, R. Wu, et al., Biosens. Bioelectron. 1790 (2021) 113062.
[43] L.M. Rao, X.Y. Lu, L.L. Xu, et al., Chemosphere 289 (2022) 133116.
[44] M.T. Stuart, N.J. Nersessian, Minds Mach. 29 (2019) 87–107.
[45] T. Mizuno, J. Appl. Probab. 43 (2016) 1181–1185.
[46] V. Quan Tran, Constr. Build. Mater. 328 (2022) 127103.